A&A 543, A5 (2012)
DOI: 10.1051/0004-6361/201219437
© ESO 2012

Astronomy & Astrophysics

The desorption of H_2CO from interstellar grains analogues

J. A. Noble[1], P. Theule[1], F. Mispelaer[1], F. Duvernay[1], G. Danger[1], E. Congiu[2], F. Dulieu[2], and T. Chiavassa[1]

[1] Aix-Marseille Univ, PIIM UMR 7345, 13397 Marseille, France
CNRS, PIIM UMR 7345, 13397 Marseille, France
e-mail: patrice.theule@univ-amu.fr
[2] LERMA-LAMAp, UMR 8112 du CNRS, Observatoire de Paris et Université de Cergy-Pontoise, 5 Mail Gay-Lussac, 95000 Cergy Pontoise, France

Received 18 April 2012 / Accepted 18 May 2012

ABSTRACT

Context. Much of the formaldehyde (H_2CO) is formed from the hydrogenation of CO on interstellar dust grains, and is released in the gas phase in hot core regions. Radio-astronomical observations in these regions are directly related to its desorption from grains.
Aims. We study experimentally the thermal desorption of H_2CO from bare silicate surfaces, from water ice surfaces and from bulk water ice in order to model its desorption from interstellar grains.
Methods. Temperature-programmed desorption experiments, monitored by mass spectrometry, and Fourier transform infrared spectroscopy are performed in the laboratory to determine the thermal desorption energies in: (i.) the multilayer regime where H_2CO is bound to other H_2CO molecules; (ii.) the submonolayer regime where H_2CO is bound on top of a water ice surface; (iii.) the mixed submonolayer regime where H_2CO is bound to a silicate surface; and (iv.) the multilayer regime in water ice, where H_2CO is embedded within a H_2O matrix.
Results. In the submonolayer regime, we find the zeroth-order desorption kinetic parameters $\nu_0 = 10^{28}$ mol cm^{-2} s^{-1} and $E = 31.0 +/- 0.9$ kJ mol^{-1} for desorption from an olivine surface. The zeroth-order desorption kinetic parameters are $\nu_0 = 10^{28}$ mol cm^{-2} s^{-1} and $E = 27.1 +/- 0.5$ kJ mol^{-1} for desorption from a water ice surface in the submonolayer regime. In a H_2CO:H_2O mixture, the desorption is in competition with the $H_2CO + H_2O$ reaction, which produces polyoxymethylene, the polymer of H_2CO. This polymerization reaction prevents the volcano desorption and co-desorption from happening.
Conclusions. H_2CO is only desorbed from interstellar ices via a dominant sub-monolayer desorption process ($E = 27.1 +/- 0.5$ kJ mol^{-1}). The H_2CO which has not desorbed during this sub-monolayer desorption polymerises upon reaction with H_2O, and does not desorb as H_2CO at higher temperature.

Key words. astrochemistry – molecular processes – ISM: molecules – molecular data

1. Introduction

Formaldehyde (H_2CO) is one of the most abundant molecules in the icy mantle covering interstellar grains. Its abundance with respect to water ice varies from 1% to 6% in high- (Keane et al. 2001; Dartois 2005) or low- (Boogert et al. 2008) mass protostars, or hot corinos (Maret et al. 2004). It is believed that CO is hydrogenated on the surface of amorphous solid water (ASW) or in bulk ASW ice to form H_2CO, which is further hydrogenated to form CH_3OH (Hiraoka et al. 1994; Watanabe & Kouchi 2002; Fuchs et al. 2009). Gas-phase H_2CO is predominantly detected in hot cores, where interstellar ice is warmed up and H_2CO sublimes (Wootten et al. 1996). A good description of desorption processes is of particular importance in hot cores regions. In these regions, the grains are being warmed during the evolution towards the main sequence. Thus hot cores are richer than quiescent molecular clouds in gas-phase saturated organic molecules (Nomura & Millar 2004). These evaporated gas-phase molecules provide a record of both the accretion taking place during the collapse phase of star formation and of the solid-state chemistry that occurs within the ice mantle. A comprehensive knowledge of both solid-state processes and sublimation processes is necessary in order to interpret hot-core observational data and to constrain star formation models. Moreover, we need to know which molecular species will remain on the grain surface after the water ice desorption, to understand which species may participate in a solid-state water-free chemistry, leading to the formation of the complex organic molecules which are detected in meteorites (Cronin & Pizzarello 1983). These refractory molecules constrain the initial abundances of this water-free chemistry that may lead to precursors of biomolecules.

Comprehensive studies of the desorption of small molecules have been made, enabling the identification of four distinct stages during the process of the desorption of molecules from interstellar grains (Collings et al. 2004, 2003a,b; Burke & Brown 2010; Noble et al. 2012): (a.) the monolayer desorption, that corresponds to the desorption of less than one layer of molecules from a surface; (b.) the multilayer desorption, corresponding to the desorption of several layers of molecules from a surface; (c.) the "molecular volcano" event (Smith et al. 1997), that corresponds to the phase transition between amorphous and crystalline ice, in the course of which molecules of other molecular species are expelled from the water ice; (d.) the co-desorption, corresponding to the dominant water desorption, when the trapped species desorb along with the ice mantle (Collings et al. 2004). Each process has its own desorption energy, and the desorption of interstellar-relevant molecules needs to be modelled taking into account their desorption characteristics,

as determined from laboratory experiments (Viti et al. 2004). According to Collings et al. (2004), molecular species can be ranked into three categories: (i.) water-like species, which co-desorb with water; (ii.) CO-like species, which show a multilayer desorption, a monolayer desorption, a volcano desorption and a co-desorption; and (iii.) intermediate species, which show the volcano desorption, the co-desorption and sometimes the monolayer desorption.

The study of a molecule's desorption characteristics is coupled with the chemical nature and the structure of the substrate itself. The adsorbate can desorb from either a bare grain surface, composed of amorphous silicate or carbonaceous material (Draine 2003), or from its icy mantle. Ice analogues grown from water vapour deposition onto a surface at 15 K are believed to be microporous (Mayer & Pletzer 1986), as evidenced by the presence of a vibrational band attributed to O-H dangling bonds on the pore surfaces at 2.73 microns (3360 cm^{-1}) (Rowland et al. 1991). However, the porosity of the ice mantle on grains in cold molecular interstellar clouds is still a matter of controversy. No dangling bond absorptions have been detected in the infrared spectra of interstellar ices (Keane et al. 2001), which means that the ice is non-porous. Laboratory studies suggest that the porosity of ice mantles could be reduced by cosmic rays impacts (Palumbo 2006; Raut et al. 2008), by UV photon irradiation (Palumbo et al. 2010) or by hydrogen atom bombardment (Accolla et al. 2011), as the grains are constantly processed in the interstellar medium. These laboratory studies suggest that under interstellar conditions, the ice mantle is amorphous and non-porous. Thermally induced segregation can also occur within the ice mantle (Öberg et al. 2009), which can change the energy with which the adsorbate is bound to the substrate.

The aim of this paper is to address how to model the thermal desorption of the formaldehyde molecule H_2CO in a robust and reliable way, complementing the work of Collings et al. (2004), taking into account the complexity of the thermal desorption processes indicated by laboratory data. We study the thermal desorption processes of formaldehyde (H_2CO) from a modeller's point of view. H_2CO is an interesting benchmark molecule since there is a wealth of radio-observations available in different interstellar environments, and especially in hot cores regions (Wootten et al. 1996). Since H_2CO originates from grain surface chemistry, its observed abundances are directly related to its desorption processes and they offer an indirect way to test H_2CO grain chemistry. The desorption processes can be thermal or non thermal, such as the photodesorption process which has recently been demonstrated in the Horsehead photon-dominated region (Guzmán et al. 2011). The Raman spectral characteristics of H_2CO hydrates (H_2CO within cages of clathrates) in ASW have been previously studied by Chazallon et al. (2008). This study establishes the link between the adsorbate and the substrate, as well as the formation of two crystalline H_2CO-H_2O hydrate phases and the desorption of H_2CO during the crystallisation of ice.

We study the H_2CO thermal desorption processes in different experimental environments: (i.) the multilayer regime, where H_2CO is bound to other H_2CO molecules; (ii.) the submonolayer regime where H_2CO is bound to a water ice surface; (iii.) the submonolayer regime where H_2CO is bound to a silicate surface; and (iv.) the mixed multilayer regime in water ice where H_2CO is embedded within a H_2O matrix. For each environment, we qualitatively observe the relative proportions of H_2CO desorbing via the different desorption processes, and we discuss how, based upon such experimental data, it is possible to retrieve desorption parameters – such as desorption energies and desorption rate pre-exponential factors – that can be easily integrated into existing gas-grain models. The last environment; (iv.), demonstrates the competition between the desorption process and the reaction of H_2CO in the presence of H_2O. At a slow temperature ramp, as exhibited in the interstellar medium, the reaction H_2CO+H_2O is dominant and all the H_2CO is transformed into polyoxymethylene (POM or polyformaldehyde), the polymer of H_2CO, which is more refractory than H_2O. Polyoxymethylene could provide an extended source of H_2CO at the higher temperature observed in comets, and a H_2CO reservoir for prebiotic chemistry (Milam et al. 2006).

2. Experiments

The desorption experiments of H_2CO in a multilayer regime (Sect. 3.1), and of H_2CO mixed with H_2O (Sect. 3.3), were performed in Marseille on the RING experimental set-up (Theule et al. 2011). Briefly, a gold plated copper surface is maintained at low temperature using a closed-cycle helium cryostat (ARS Cryo, model DE-204 SB, 4 K cryogenerator) within a high-vacuum chamber at a few 10^{-9} mbar. H_2O is outgassed into a vacuum line using standard manometric techniques. H_2CO is obtained by gently warming paraformaldehyde. Molecular solids samples are formed by spraying the room-temperature gas onto the gold surface. Porous, amorphous ice analogues are grown by depositing water vapour onto the gold surface held at 15 K. Amorphous, non-porous (or compact) ice analogues are grown by depositing water vapour onto the surface between 90 K and 130 K. Such a compact ASW ice has no or little porosity, which prevents the trapping of molecules in pores.

The infrared spectra are recorded by means of Fourier-transform reflection absorption infrared Spectroscopy (FT-RAIRS) using a Vertex 70 spectrometer with either a DTGS detector or a liquid N_2 cooled MCT detector. A typical spectrum has a 1 cm^{-1} resolution and is averaged over a few hundred interferograms. The sample temperature is measured with a DTGS 670 Silicon diode with a 0.1 K uncertainty. The temperature is controlled using a Lakeshore Model 336 temperature controller and a heating resistance. A Hiden HAL VII RGA quadrupole mass spectrometer (QMS) measures desorbing gas-phase species. In a typical temperature-programmed desorption experiment (TPD), the mass spectra are recorded with the QMS as the products are being desorbed from the surface, heated by a 4 K/min temperature ramp. The concentration ratio of the deposited molecular solids is derived from their IR spectra right after deposition. For each molecule, the characteristic bands are integrated, and then divided by their corresponding band strengths to estimate their column densities (molecules cm^{-2}). For H_2O, we use the values of 3.1×10^{-17} cm molecule^{-1} for the band strength of the libration mode at 760 cm^{-1} and 1.2×10^{-17} cm molecule^{-1} for the band strength of the OH bending mode at 1670 cm^{-1} (Gerakines et al. 1995). For H_2CO we use the CO stretching mode band at 1721 cm^{-1}, which has a band strength of 9.6×10^{-18} cm molecule^{-1} (Schutte et al. 1996). A 30% uncertainty on the band strengths, and therefore on calculated column densities, is probably conservative enough.

The H_2CO desorption experiments in the sub-monolayer regime (Sect. 3.2) were performed in Cergy-Pontoise using the FORMOLISM experimental set-up (Amiaud et al. 2006). Briefly, the apparatus consists of an ultra-high vacuum stainless steel chamber, with base pressure in the low 10^{-10} mbar range, containing an amorphous silicate-coated gold surface (5–400 K)

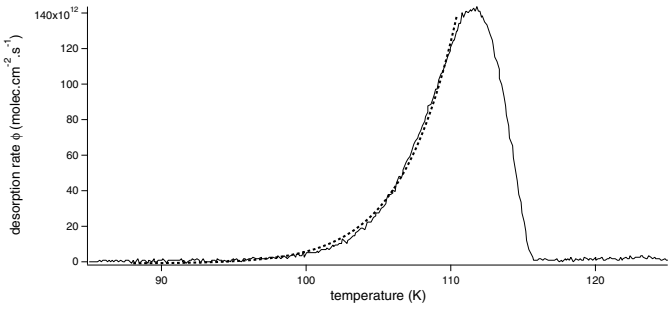

Fig. 1. Quadrupole mass spectrometer temperature-programmed desorption curve (m/z 30) of a pure H_2CO multilayer sample heated at a 4 K/min temperature ramp rate. The desorption rate has been normalised to a one monolayer coverage (10^{15} molec cm^{-2}). The dashed line is the result of fitting the experimental data with a zeroth-order Polanyi-Wigner equation (Eq. (1)).

(Noble et al. 2012). The silicate is a San Carlo olivine, deposited using a physical vapour deposition technique. The compact and non-porous water ice substrate (100 monolayers) is grown on the silicate (held at 110 K) by spraying water vapour from a microchannel array doser, then cooled down to 10 K before beginning the experiments. H_2CO is formed from CO hydrogenation experiments in a low coverage regime. The temperature is measured with a calibrated silicon diode clamped on the sample holder and controlled by computer to ±0.2 K with an accuracy of ±1 K in the 8−400 K range.

Reactants are introduced into the vacuum chamber via two separate triply differentially pumped beam lines aimed at the cold surface. The first beam line is used to deposit CO with a flux that was previously calibrated using temperature-programmed desorption by determining the CO exposure time required to saturate the CO monolayer on compact ice (Kimmel et al. 2001). The second beam line is used to introduce H atoms. Desorption of molecules from the surface is monitored using a quadrupole mass spectrometer positioned directly in front of the surface.

3. Results

3.1. Desorption of pure H_2CO in the multilayer regime

These experiments were performed on the RING experimental set-up. Pure H_2CO is deposited at 15 K on the gold surface to obtain a multilayer sample of H_2CO. Using the column density derived from the IR band at 1721 cm^{-1}, we can estimate that the sample thickness is approximately 50 monolayers. The solid H_2CO sample is submitted to a 4 K/min temperature ramp. The TPD curve of H_2CO given by the QMS signal exhibits a zeroth-order thermal desorption pattern, characteristic of bulk desorption in the multilayer regime (Redhead 1962; Carter 1962), as shown in Fig. 1. Depositing two different quantities of H_2CO results in TPD curves with a similar rising edge and two different sharply falling edges.

The measured QMS signal is proportional to the instantaneous desorption rate; the coefficient of proportionality is related to both the collection efficiency and the ionisation yield of the QMS spectrometer. The desorption rate φ is normalised to a one monolayer coverage (10^{15} molec cm^{-2}) and to a 1 cm^2 surface by dividing by the integral of the QMS curve and multiplying by 10^{15} molec cm^{-2} × 1 cm^2. We fit the rising edge of the normalised desorption rate φ curve with a zeroth-order of the Polanyi-Wigner equation, as a function of temperature T (Redhead 1962; Carter 1962):

$$\varphi(T) = -\frac{\mathrm{d}N}{\mathrm{d}T} = \frac{\nu_0}{\beta} \times \exp\left(-\frac{E}{R \times T}\right), \quad (1)$$

where N is the surface coverage (molecules cm^{-2}), ν_0 is the zeroth-order pre-exponential factor of the rate constant, E is the desorption energy, R is the ideal gas constant, and β the temperature ramp rate (β = 1/15 K s^{-1} in our case). Since ν_0 and E are correlated, we can obtain a non physically relevant E by adjusting both ν_0 and E on the TPD curve. Instead, we choose to fix ν_0 to a physically relevant value, in order to compare the desorption energies of different molecules. So we fix ν_0 to 10^{28} molec cm^{-2} s^{-1} using a typical 10^{15} molec cm^{-2} surface density of sites and a typical 10^{13} s^{-1} adsorbate-surface oscillation frequency. Both values can change by a factor of a few, according to the nature of the adsorbed molecule and of the surface. The surface coverage is related to the average distance between two adsorption sites, and the oscillation frequency to the nature of the interaction between the surface and the adsorbate. The uncertainty in ν_0 is directly correlated to the derived value of E.

Fitting the rising edge of the TPD curve with only E as a free parameter and fixing $\nu_0 = 10^{28} \pm 0$ molec cm^{-2} s^{-1}, we obtain $E = 31.3 \pm 0.5$ kJ mol^{-1} for the multilayer desorption of pure H_2CO. The ±0.5 kJ mol^{-1} uncertainty on E is the dispersion of E from different TPD experiments. The uncertainty on the fit itself or on choosing different portion of the rising edge of the TPD curve gives an approximate 0.03 kJ mol^{-1} uncertainty on E. With both ν_0 and E as free parameters, we obtain $\nu_0 = (2.3 \pm 0.1) \times 10^{27}$ molec cm^{-2} s^{-1} and $E = 30.0 \pm 0.4$ kJ mol^{-1}. Varying the oscillation frequency from 10^{12} s^{-1} to 10^{14} s^{-1} gives a ±2 kJ mol^{-1} spread on E. So we choose to use the coupled solution $\nu_0 = 10^{28} \pm 0$ molec cm^{-2} s^{-1}, $E = 31.3 \pm 0.5$ kJ mol^{-1} to express the zeroth-order desorption rate of multilayer H_2CO. The value of the pre-exponential factor is an important parameter to take desorption into account. Its value must be specified alongside the desorption energy in astrochemical models, and not arbitrarily fixed or independently calculated, only taking the experimentally measured desorption energy as input.

3.2. Desorption of H_2CO in the sub-monolayer regime

The submonolayer experiments were performed on the FORMOLISM set-up. Temperature programmed desorption experiments are performed with H_2CO in the sub-monolayer regime, i.e. $H_2CO \leq 10^{15}$ mol cm^{-2}. $H_2^{13}CO$ is produced by the hydrogenation of one layer of ^{13}CO deposited on top of either a compact amorphous ice or a silicate surface. In both cases, two experiments are performed, bombarding the ^{13}CO surface with H atoms for 30 min and 45 min respectively, which corresponds to a fluence of 1.8 × 10^{16} and 2.4 × 10^{16} H atoms cm^{-2} respectively. In our conditions, TPD spectra show that CH_3OH is formed at a level less than 1% (Fuchs et al. 2009; Watanabe & Kouchi 2002). Then, the remaining ^{13}CO and the $H_2^{13}CO$ irradiation product are submitted to a 0.04 K s^{-1} temperature ramp and they desorb. Figure 2 shows the m/z 31 TPD curve for the desorption of the $H_2^{13}CO$ sub-monolayer on a compact amorphous ice surface and of a silicate surface.

3.2.1. Desorption of H_2CO in the sub-monolayer regime on an ASW surface

H_2CO desorption in the sub-monolayer regime on a compact non-porous amorphous ice surface (deposited at 110 K and cooled down to 10 K) can be fitted by first-order desorption kinetics, which is typical of sub-monolayer desorption. The

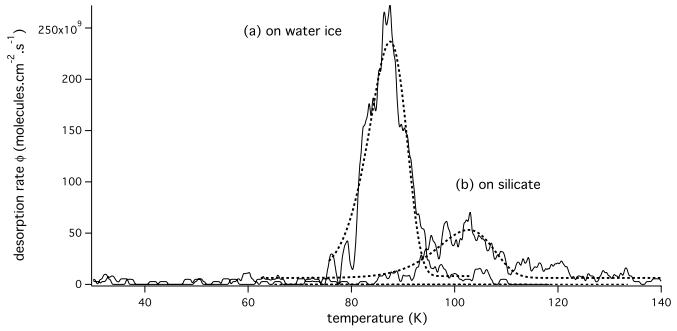

Fig. 2. Temperature-programmed desorption curves (m/z 31, 0.04 K s^{-1} temperature ramp rate) of a sub-monolayer of $H_2^{13}CO$ on **a)** a compact amorphous H_2O surface and **b)** a silicate surface. The dashed lines are the results of fitting the experimental data with a first-order Polanyi-Wigner equation.

instantaneous desorption rate $\varphi(T)$ as a function of temperature T for first-order kinetics is given by (Redhead 1962):

$$\varphi(T) = -\frac{\mathrm{d}N}{\mathrm{d}T} = \frac{\nu_1}{\beta} \times N \times \exp\left(-\frac{E}{R \times T}\right), \quad (2)$$

where N is the surface coverage (molecules cm^{-2}), ν_1 is the first-order pre-exponential factor of the rate constant, E is the desorption energy, and R the ideal gas constant.

At temperature T_p, the desorption rate $\varphi(T)$ is at its maximum, and Eq. (2) can be derived:

$$\frac{E}{R \times T_\mathrm{p}^2} = \frac{\nu_1}{\beta} \times \exp\left(-\frac{E}{R \times T_\mathrm{p}}\right). \quad (3)$$

We fit the experimental TPD curves in three different ways. The different uncertainties are determined from the spread by taking m/z 30 and m/z 31 for the two different experiments, with 30 min and 45 min H bombardment respectively.

First, following Redhead (1962), we can obtain from Eq. (2) the equation describing the shape of the first-order desorption rate curve:

$$\ln\left(\frac{N_\mathrm{p}}{N}\right) = \frac{E}{R}\left(\frac{1}{T_\mathrm{p}} - \frac{1}{T}\right) + \left(\frac{T}{T_\mathrm{p}}\right)^2 \exp\left(-\frac{E}{R}\left(\frac{1}{T} - \frac{1}{T_\mathrm{p}}\right)\right) - 1, \quad (4)$$

where N_p is the surface coverage at the temperature where the desorption rate is at its maximum (T_p).

The experimental TPD curves are fitted with Eq. (4), which gives T_p and the desorption energy $E = 15.0 +/- 1.5$ kJ mol^{-1}. With these values for T_p and E, Eq. (3) gives $\nu_1 = 2 \times 10^{5+/-1}$ s^{-1}. Once again, the correlation between E and ν_1 prevents us from deriving accurate values for these two parameters.

An alternative method is to fix $\nu_1 = 10^{13}$ s^{-1} and to take the maximum desorption rate temperature T_p determined from the fit of the TPD curve with Eq. (4). This determination of T_p is slightly more accurate than simply taking the maximum of the TPD curve. We then solve Eq. (3) with these values for ν_1 and T_p to find $E = 25.0 +/- 0.1$ kJ mol^{-1}. $\nu_1 = 10^{13}$ s^{-1} and $E = 25.0 +/- 0.1$ kJ mol^{-1} are physically more realistic values (lying between the values of 14.5 kJ mol^{-1} for CO (Burke & Brown 2010) and 46.6 kJ mol^{-1} for H_2O (Fraser et al. 2001)), and the pair of parameters well reproduces the overall desorption rate.

Finally, we can also fit the TPD curve using a zeroth-order Polanyi-Wigner equation, as expressed in Eq. (1), fixing $\nu_0 = 10^{13}$ s^{-1} $\times$ 10^{15} mol cm^{-2} = 10^{28} mol cm^{-2} s^{-1}. We find $E = 27.1 +/- 0.5$ kJ mol^{-1}. So, we see that the values of the desorption energies derived upon assuming zeroth- or first- order desorption kinetics differ by approximately 4%. However, using Eq. (1) or Eq. (2), with either $\nu_0 = 10^{28}$ mol cm^{-2} s^{-1} or $\nu_1 = 2 \times 10^{5+/-1}$ s^{-1}, makes a significant difference when applied within gas-grain models. *Thus, it is important to take the correct couple of solution (ν, E) when inputing experimental data in models.*

3.2.2. Desorption of a H_2CO in the sub-monolayer regime on a silicate surface

We follow the same procedures to extract the desorption parameters from the TPD curves of the H_2CO desorption in the sub-monolayer regime on a silicate surface. Silicate surfaces are representative of grain bare surfaces during the transition from diffuse to molecular clouds. We find $\nu_1 = 10^{13 \pm 0}$ s^{-1} and $E = 29.2 +/- 0.9$ kJ mol^{-1} assuming first-order desorption kinetics and $\nu_0 = 10^{28}$ mol cm^{-2} s^{-1}, and $E = 31.0 +/- 0.9$ kJ mol^{-1} assuming zeroth-order desorption kinetics. As for the ASW surface, on the silicate surface, the derived desorption energies differ by only few percent. As expected, H_2CO is more tightly bound on a silicate surface than on a water ice surface.

3.3. Interaction of H_2CO with ASW

We now want to further investigate how a water ice environment affects the desorption of a simple hydrogen-bound molecule such as H_2CO. To do this we perform three types of experiments. In the first type, several layers of H_2CO are deposited on top of a thick water ice film to investigate how the ASW substrate affects the H_2CO multilayer desorption seen in Sect. 3.1. In the second, several layers of H_2O are deposited on top of a solid H_2CO film. In the third, H_2CO is mixed in the gas phase with H_2O and deposited as an homogeneous film. This latter scenario is probably the closest to the interstellar ice morphology, if one assumes that CO is hydrogenated into H_2CO during the mantle build-up, which is therefore homogeneously mixed with H_2O in the inner polar component of the interstellar ice. Figure 3 shows the IR spectra of the three types of H_2CO ice mixtures immediately after deposition at 15 K. We can see from this spectrum that, upon deposition, the ν_{CO} band of H_2CO is located at 1720 cm^{-1}, which is characteristic of a solid-state H_2CO:H_2O mixture (Schutte et al. 1993). For each mixture, the H_2CO:H_2O concentration ratio is obtained from the integration of their IR absorption bands as described in Sect. 2. The H_2CO:H_2O mixtures are deposited either on a 15 K or a 90 K gold surface to obtain either a porous or a non-porous compact ice, in order to understand how the ice morphology may affect our results. The H_2CO:H_2O ice mixture TPD curves exhibit several desorption features that we label M (multilayer desorption from the surface of water ice), V (volcano) and C (co-desorption with H_2O) following the designation in Collings et al. (2004).

3.3.1. Desorption of H_2CO on top of ASW

We deposit a film of H_2CO on top of a porous ASW film at 15 K with an abundance ratio of 1/14 between the H_2CO/H_2O layers. The ASW film is deposited first, and then the H_2CO film is deposited at the same temperature on top of it. A temperature-programmed desorption experiment is performed on the H_2CO/H_2O layered system, which exhibits M and V desorption features, as seen in Fig. 4.

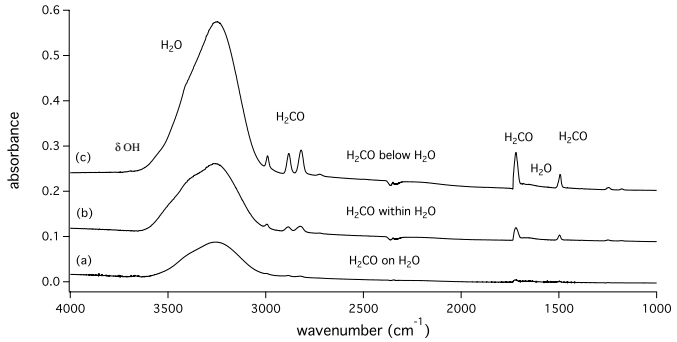

Fig. 3. IR spectra of three H_2CO:H_2O ice mixtures at 15 K. The concentration ratio of each species in the mixture is determined from the integration of its characteristic IR bands. Mixture **a)** is a layered system where H_2CO is on top of H_2O, mixture **b)** is an homogeneous mixture of H_2CO:H_2O, and mixture **c)** is a layered system where H_2O is on top of H_2CO. The observation of small bands at around 3700 cm^{-1}, attributed to dangling OH, δ_{OH}, confirms that the ASW deposited at 15 K is porous.

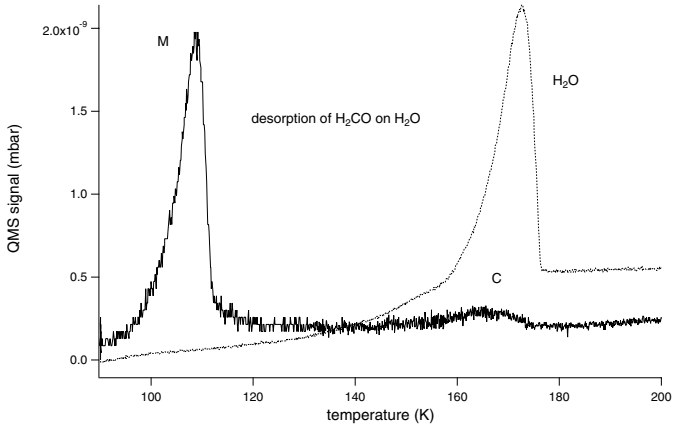

Fig. 4. Temperature-programmed desorption curves (m/z 30, 4 K min^{-1} temperature ramp rate) of a H_2CO/H_2O layered system where a H_2CO film is on top of a H_2O film (1/14 H_2CO/H_2O abundance ratio). Two features, labelled M and C on the TPD curve, correspond to the multilayer and co-desorption with water (m/z 18 in dashed line), respectively.

As expected, the M feature corresponds to the multilayer regime desorption, as described in Sect. 3.1, of the H_2CO bounded to other H_2CO molecules by van der Waals interactions. The weak C feature corresponds to the co-desorption of H_2CO molecules trapped within the H_2O network. This corresponds to the physisorption of H_2CO to surrounding H_2O molecules, and to a trapping of H_2CO molecules in the form of hydrates (Chazallon et al. 2008). The presence of H_2CO molecules trapped within the ice indicates that the H_2CO molecules have penetrated from the surface into the first monolayers of ASW. This is evidence that H_2CO can diffuse downwards in ASW and that an appreciable quantity of it can be trapped within the ice as hydrates, which co-desorb with the bulk of the ice mantle. This co-desorption phenomenon is different to the desorption of adsorbed H_2CO on an ASW surface as studied in Sect. 3.2.1, and has a desorption energy similar to that of H_2O, which has a 48 kJ mol^{-1} desorption energy (Fraser et al. 2001) and is expected to desorb in this temperature range, as shown in Fig. 5d.

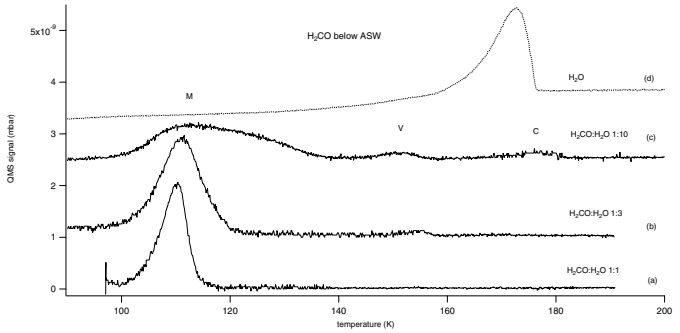

Fig. 5. Temperature-programmed desorption curves (m/z 30) of three H_2O/H_2CO layered systems where an ASW film is on top of a H_2CO film in varying H_2O/H_2CO abundance ratios: **a)** 1/1, **b)** 3/1 and **c)** 10/1. The M, V and C features are visible on the TPD curves. **d)** TPD curve (m/z 18) of H_2O (scaled × 0.125).

3.3.2. H_2CO below ASW

To illustrate the diffusion of H_2CO within ASW, and its relationship with desorption, we deposit an ASW film on top of a H_2CO film in order to form a H_2O/H_2CO layered system where H_2CO has to diffuse to reach the surface and desorb. First the H_2CO film is deposited at 15 K, and then H_2O is deposited at the same temperature on top of the H_2CO film. The TPD curves of three layered systems with different H_2O/H_2CO abundance ratios are displayed in Fig. 5.

During the TPD experiments, H_2CO must diffuse through the bulk of ASW in order to reach the ASW surface, and then to desorb to be detected by the QMS. When the ASW film is thin, as in layered system (a), the TPD curve is similar to the pure formaldehyde desorption TPD curve (Fig. 1). No V and C features are observed for H_2CO under a thin ASW film. As the ASW film thickness increases, the monolayer desorption M feature broadens and shifts to higher temperature, as seen in Fig. 5 for layered systems (b) and (c). The broadening of the M feature is due to the time delay necessary for the H_2CO molecules to diffuse in the ASW film, and this delay increases with ASW thickness. The V feature is visible in layered systems (b) and (c), but not in layered system (a). As expected, the thicker the ASW film, the more H_2CO is trapped. The C feature is visible for the thickest ASW film, layered system (c). These three experiments illustrate that the diffusion of H_2CO through an ASW film, firstly, slows down the desorption and, secondly, allows the trapping of H_2CO molecules within the ASW ice; the thicker the ice film, the more pronounced the slowing and trapping effects. We can observe that in a TPD experiment, the trapping within closed pores during pore collapse (the V feature, Smith et al. 1997), occurs at a lower dilution than the trapping by the formation of hydrates (the C feature), as seen by comparison of the (b) and (c) layered systems. The molecular volcano desorption and co-desorption must be taken into account in gas-grain models, as done in Viti et al. (2004), although it is difficult to account quantitatively of the relative proportion of each desorption process. Interstellar grains are thinner than our laboratory ice analogues, and H_2CO is formed from homogeneously mixed CO, so we need to study more realistic ice analogues.

3.3.3. Diffusion and reactivity of H_2CO within ASW

To better understand the relationship between H_2CO and H_2O in an ice analogue closer to an interstellar ice, we performed experiments on thinner, homogeneously mixed, and diluted H_2CO:H_2O ice mixtures, with a typically 1−2% concentration

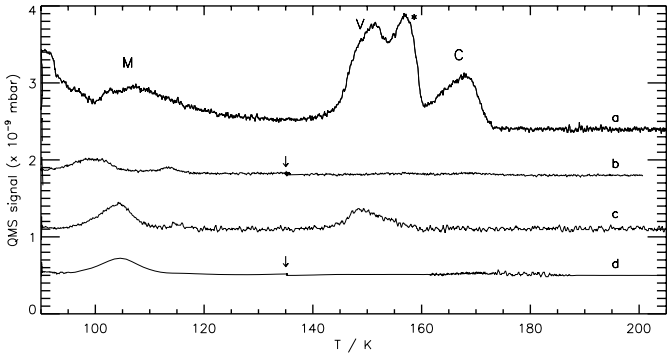

Fig. 6. TPD spectra (m/z = 30) for the H_2CO:H_2O mixtures, **a)** 1:14 deposited at 15 K, heated at 2 K min^{-1} 90−210 K, **b)** 1:8 deposited at 15 K, heated at 2 K min^{-1} 90−135 K, held at 135 K for 14.5 h, heated at 2 K min^{-1} 135−210 K, **c)** 1:6 deposited at 90 K, heated at 2 K min^{-1} 90−210 K, **d)** 1:9 deposited at 90 K, heated at 2 K min^{-1} 90−135 K, held at 135 K for 18 h, heated at 2 K min^{-1} 135−210 K. The arrows indicate that an isothermal break of several hours was made in the TPD experiment. M, V, and C correspond to the multilayer, the volcano and co-desorption desorptions, respectively. The asterisk indicates a double peaked structure, observed as a result of desorption of H_2CO from the radiation shield.

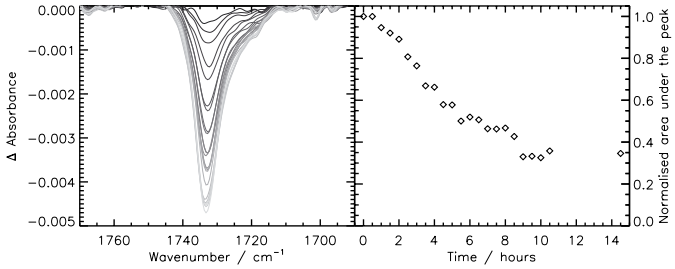

Fig. 7. *Left hand panel*: difference spectra of the H_2CO stretching mode absorption at 1735 cm^{-1} while the surface is held at 135 K. These data correspond to trace b in Fig. 6. Black corresponds to time =0, light grey corresponds to time =14.5 h. *Right hand panel*: these data are the calculated area under the peak for the same absorption band, plotted as a function of time held at 135 K.

ratio. To do so we deposited a gas-phase mixture of H_2CO and H_2O on the gold surface to obtain homogeneous porous H_2CO:H_2O mixtures with varying concentration ratios, both at 15 K (porous ASW) and at 90 K (compact ASW). As with previous experiments, the concentration ratios for the two H_2CO:H_2O mixtures are obtained from their IR spectra, right after deposition. The spectra are shown in Fig. 3.

In a first experiment (a), a gas-phase mixture of H_2CO:H_2O with a 1:14 concentration ratio was deposited at 15 K. The mixture was heated to 90 K at a rate of 10 K min^{-1}; it was then heated at 2 K min^{-1} between 90 and 210 K. The TPD spectrum for mass 30 is shown in Fig. 6, trace (a). As in Fig. 5c, peaks M, V, and C (corresponding to the multilayer regime, volcano and co-desorption regimes, respectively) are visible in the trace.

In another experiment (b), a similar ice mixture (1:8 concentration ratio) was deposited at 15 K, heated rapidly (10 K min^{-1} temperature ramp rate) to 90 K and then heated at 2 K min^{-1} to 135 K. To simulate experimentally the slow temperature ramp rates in the interstellar medium (*c.a.* 1 K century^{-1} in hot core regions, Viti & Williams 1999), we maintained the ice at a temperature intermediate between the multilayer M desorption and the volcano desorption, V, for an extended period of time. The ice mixture was held at 135 K for 15 h, after which the surface was heated at 2 K min^{-1} from 135 to 200 K. The only difference between the two experiments was that the temperature was held at 135 K for 15 h during the second experiment. The TPD spectrum of mass 30 for the second experiment is shown in Fig. 6b. In this trace, the multilayer desorption, M, is still evident, but there is no peak corresponding to desorption from a volcano regime, nor in a co-desorption regime.

These two experiments were repeated, with deposition of the H_2CO:H_2O mixtures at 90 K, rather than 15 K, to investigate the effect of a more compact morphology of the ASW ice on the desorption. In experiment (c), the 2 K min^{-1} TPD experiment is uninterrupted from 90 K to 200 K (as in experiment (a)), while in experiment (d) the TPD experiment is interrupted (as in experiment (b)), with the ice mixture being held at 135 K for 18 h before resuming the TPD experiment. As seen in Fig. 6, again, no volcano or co-desorption peak is seen in the interrupted experiment (trace (d)).

During the interruption period at 135 K in experiment (b), infrared spectra were taken at 30 min intervals. Study of the evolution of the IR spectra with time at the fixed 135 K temperature shows that, during the interruption, the H_2CO CO stretching mode absorption band at 1735 cm^{-1} disappears, while several IR bands appear in the spectra. Figure 7, left panel, shows the time evolution of the difference spectra of the 1735 cm^{-1} H_2CO CO stretching mode absorption over 15 h. On the right panel, the area under the ν_{CO} H_2CO absorption band has been plotted as a function of time held at 135 K. It is evident from this figure that the abundance of H_2CO in the ice mixture has decreased during the time that the surface is held at 135 K. After 15 h at 135 K, it has not fully disappeared 100%. It is interesting to note that the ν_{CO} band can be deconvolved into two separate components: a small component at 1720 cm^{-1} corresponding to H_2CO in ASW and a dominant component at 1735 cm^{-1}. The position of the ν_{CO} band at 1735 cm^{-1} indicates the presence of H_2CO hydrates (Chazallon et al. 2008). This confirms that, when in ASW, H_2CO molecules are trapped in clathrates.

The bands which appear in the infrared spectrum of the H_2CO:H_2O mixture during the interruption can be assigned to polyoxymethylene (POM) (Schutte et al. 1993). Figure 8 compares the IR spectra of the interrupted experiment at 215 K, when all the H_2CO has desorbed via the desorption regimes detailed above, with a reference spectrum for the POM. The reference spectrum was obtained from a H_2CO:H_2O:NH_3 ice mixture (an excess of H_2CO with respect to NH_3 in a H_2O dominant ice) following the methodology of Schutte et al. (1993). The agreement between the two spectra shows that we have formed POM. Compared to the POM reference spectrum (Fig. 8d), an excess in the OH band, between 3300 and 3500 cm^{-1}, is evident in our experimental spectrum at 215 K (Fig. 8c). This excess indicates the production of short CH_2-O-$_n$ chains, which results in an enhanced proportion of OH to CH groups located in the polymer chains.

This IR study shows that the H_2CO trapped in the ASW ice has polymerised to form short chain polymers of the type -CH_2-O-$_n$, called polyoxymethylene. Because we are working in a diluted H_2CO:H_2O ice mixture, with 1−2% H_2CO, this means that H_2CO monomers have diffused within the ASW ice, become trapped, and then concatenated to form POM. Such a polymerisation reaction is not observed in a pure H_2CO solid. This confirms experiments carried out in Sect. 3.3.2 on the ability of H_2CO to diffuse within ASW. However, one may imagine that, as in the experiments in Sect. 3.3.2, H_2CO would diffuse, reach the surface, and then desorb, rather than becoming trapped and polymerising. To evaluate the proportion of initial

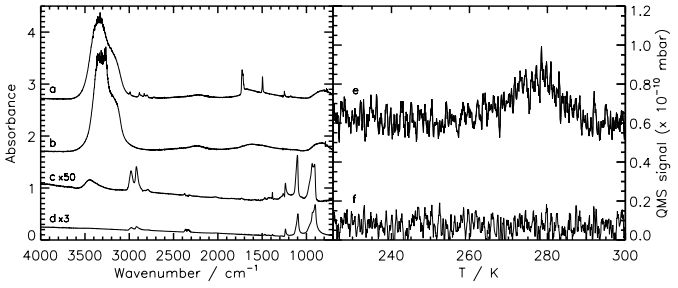

Fig. 8. Spectra of polyoxymethylene (POM, -CH_2-O-$_n$). *Left hand panel*: IR spectra **a)** IR spectrum taken at 100 K (H_2CO:H_2O mixture deposited at 90 K). **b)** an IR spectrum taken at 145 K during the same TPD. **c)** an IR spectrum taken at 215 K. **d)** a reference spectrum of POM taken at 300 K. *Right hand panel*: mass spectra **e)** m/z 30. **f)** m/z 60.

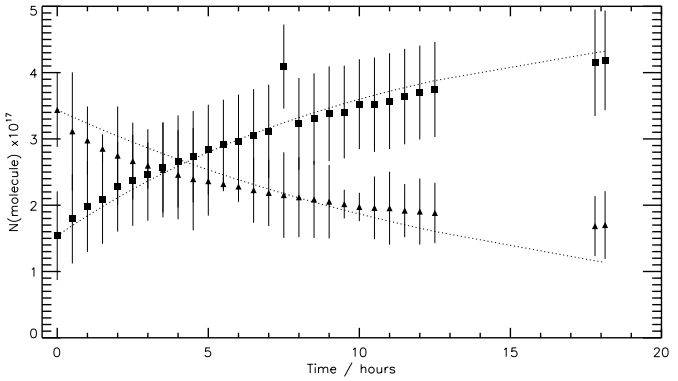

Fig. 9. Time evolution of the H_2CO and POM abundances (with error bars) at 135 K, as derived from their integrated IR absorption bands. An $A = 1.9 \times 10^{-18}$ cm molec^{-1} band strength is chosen for the 1100 cm^{-1} band (Schutte et al. 1993).

H_2CO that reacts and the proportion of H_2CO that escapes in the gas phase, we compare the kinetics of the reaction of H_2CO and production of POM in Fig. 9. As H_2CO is highly diluted into ASW, we can fit these curves with first-order reaction kinetics, and we obtain $1.69(7) \times 10^{-5}$ s^{-1} for the H_2CO destruction rate and $2.5(1) \times 10^{-5}$ s^{-1} for the POM formation rate. These two rates are comparable. Moreover, when we calculate the number of molecules of each species, we obtain approximately 3.5×10^{17} molecules of H_2CO (initial concentration) and 4×10^{17} molecules of POM (final concentration), taking the band strength from Schutte et al. (1993). Therefore, we can conclude that the initial H_2CO present in the ice mixture mainly reacts to form the POM, and that little, if any, H_2CO escapes in the gas phase. Furthermore, the QMS signal measured during the isothermal period of experiments (b) and (d) does not indicate any H_2CO desorption, which confirms, within the observational limits of our experiments, that most of H_2CO reacts and does not desorb. POM is refractory, since it desorbs around 280 K in our experimental conditions. The solid-state H_2CO reactivity must be taken into account into gas-grain models as it lowers gas-phase quantity calculated in present models.

4. Discussion

We have illustrated in this work how the desorption of H_2CO is intrinsically linked to the ASW ice substrate. Figure 10 summarises the different desorption experiments performed on H_2CO. In the multilayer regime, bulk H_2CO ice desorbs following zeroth-order kinetics, which can

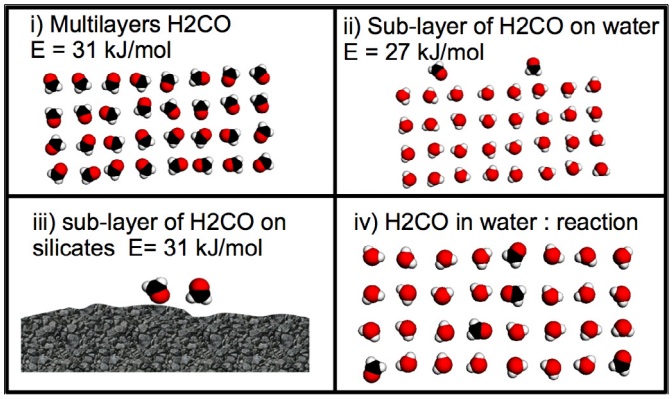

Fig. 10. Summary of the different H_2CO desorption experiments performed, including the derived desorption energies (the Arrhenius equation pre-exponential factor being fixed to 10^{28} molec cm^{-2} s^{-1}) of each experiment. (i.) H_2CO multilayer sample; (ii.) sub-monolayer of H_2CO on top of a compact amorphous ice surface; (iii.) sub-monolayer of H_2CO on top of a silicate surface; (iv.) H_2CO embedded in amorphous water ice.

be modelled using a Polanyi-Wigner equation with the parameters $\nu_0 = 10^{28} \pm 0$ molec cm^{-2} s^{-1}, $E = 31.3 \pm 0.5$ kJ mol^{-1}. In the submonolayer regime, H_2CO desorbs following first-order desorption kinetics. It is however simpler, and as accurate, to model this desorption as a zeroth-order desorption, employing the Polanyi-Wigner equation with the parameters $\nu_0 = 10^{28}$ mol cm^{-2} s^{-1} and $E = 27.1 +/- 0.5$ kJ/mol for the desorption from an ASW surface and with the parameters $\nu_0 = 10^{28}$ mol cm^{-2} s^{-1} and $E = 31.0 +/- 0.9$ kJ/mol for a silicate surface. These parameters have been obtained by fixing the pre-exponential factor, ν_0, as the physically relevant value of 10^{15} mol cm$^{-2} \times 10^{13}$ s^{-1} = 10^{28} mol cm^{-2} s^{-1}, since the pre-exponential factor and the desorption energy are correlated due to either random experimental errors (Barrie 2012a) or systematic errors (Barrie 2012b). Since the physically relevant quantity is the desorption rate only, arbitrarily fixing the pre-exponential factor to a physical value allows comparison of the desorption of two different molecules, as well as offering a robust method to implement desorption in gas-grain chemistry codes, without attributing a pre-exponential factor for each molecule on different types of surfaces. This also provides a simple way to rank molecules on a scale of desorption energy, with the desorption energy as a single parameter instead of invoking the coupled parameters, pre-exponential factor and desorption energy. Using this simple scale it it easy to determine whether one type of molecule desorbs faster or slower than another, and especially to compare its desorption with that of H_2O, i.e. to determine whether a molecule is volatile or refractory. Implementing this comparison using the values we derived in this work, we see that a H_2CO molecule which is bound by van der Waals interactions to other H_2CO molecules desorbs in the multilayer regime with an energy (31.3 ± 0.5 kJ mol^{-1}) greater than the desorption energy ($27.1 +/- 0.5$ kJ/mol) of H_2CO bound by hydrogen bonds to H_2O molecules on an ASW surface. The $31.0 +/- 0.9$ kJ/mol value for H_2CO for a silicate surface is close to the H_2CO on H_2CO value. This tells us that, either the H_2CO monomers aggregate to form clusters whose desorption value is close to that in the multilayer regime, or that silicate-H_2CO van der Waals interactions are similar in energy to H_2CO-H_2CO interactions, or that H_2CO is hydrogen bounded to a SiOH silanol group if the silicate surface is hydrated. Due to the low hydrogenation yield of H_2CO produced from CO, the latter explanation is probably more plausible.

The H_2CO desorption influenced by interaction with the ASW network is the most interesting from an astrochemical perspective, as this environment is the closest to real interstellar ice. It is also a case to study illustrating how conducting standard laboratory experiments can result in false conclusions being drawn. A standard TPD experiment of a H_2CO:H_2O mixture (of the type performed in Sect. 3.3.3, experiments (a) and (c)) may lead us to conclude that H_2CO has a multilayer regime desorption, similar to that of pure H_2CO desorption, and that, like many other molecules (CO_2, NH_3,...), a fraction of the H_2CO is trapped within the closed pore network of ASW. It is eventually released both during the volcano desorption (i.e. the pore collapse associated with the phase transition from amorphous ice to crystalline ice) and the co-desorption (when the H_2O mantle desorbs) regimes, as seen in traces (a) and (c) of Fig. 6. However, interrupting the TPD experiments at a temperature between the monolayer desorption and the volcano desorption allows the simulation of the extremely slow heating rates encountered in star formation regions (Viti & Williams 1999). Curves (b) and (d) of Fig. 6 lead to a totally different conclusion. Indeed, H_2CO molecules are trapped in the ice – either within pores or as hydrates (Chazallon et al. 2008) – and can diffuse and react with themselves in a H_2O environment (which both initiates the polymerisation reaction and lowers the reaction barrier) to form the POM polymer. In our experimental conditions, the polymerisation reaction is faster than diffusion to the surface and thus dominates the H_2CO chemistry before H_2O desorption, as well as preventing volcano desorption or co-desorption. Moreover, diffusion within the ice and trapping within the pores offer an efficient way to concentrate diluted molecules, enhancing the possibility of a rich ice chemistry. Furthermore, POM is acting as a reservoir of H_2CO, which could then be released at higher temperature in the interstellar medium, i.e. at temperatures where neither H_2CO nor H_2O would be expected to be present in the solid-phase. Other competitive reactions with low-reaction barriers, such as the reaction H_2CO + NH_3 that forms aminomethanol NH_2CH_2OH (Bossa et al. 2009), or the reaction H_2CO + $NH_4^+CN^-$ that forms hydroxyacetonitrile $HOCH_2CN$ (Danger et al., in prep.), can also occur, preventing the desorption of H_2CO.

Crucially, this work illustrates the importance of taking the diffusion process into account. There are three competitive processes: the diffusion of the H_2CO molecule – which probably leads to the formation of hydrates – within the ASW mantle; the desorption of the H_2CO molecule from the top layer of ASW (the surface); and the reactivity between H_2CO monomers. Diffusion is needed both because molecules need to reach the surface in order to desorb and because molecules need to meet for a reaction to occur. Which of the three processes is dominant depends on the interstellar grain morphology and initial abundances. In the extreme case where the grain has a radius much greater than the thickness of the ASW mantle and there is a very low initial abundance of H_2CO with respect to H_2O, the number of steps required to reach the surface in the radial direction is much smaller than the number of steps required to diffuse in the circular direction and encounter diluted potential reactants. So most of the molecules will diffuse towards the surface to desorb. At the opposite extreme, where the grain radius is small and the ice is very thick, circular diffusion will favour reactivity, which will dominate over radial diffusion and desorption processes. H_2CO is present in interstellar ices at abundances on the order of a few percent with respect to water, and the ice mantle has a typical thickness of few tens of monolayers, so radial diffusion, which is related to desorption, and circular diffusion, which is related to reactivity, are likely to be around the same order of magnitude. Within this grain-mantle system, we see that diffusion is central to correctly modelling both desorption and reactivity, as well as their competition. However, very few data exist on the diffusion of simple molecules in ice at low temperature (Livingston et al. 2002), so diffusion is currently a major issue for modelling desorption on interstellar grains.

The interstellar grain shape adopted in models is also of importance. A central conclusion drawn from this study is that there is no easy answer to the question of how to correctly model the desorption of H_2CO from ice mantles. If using a multilayer grain chemistry model, one can consider that the value of $E = 27.1 +/- 0.5$ kJ/mol for the H_2CO desorption from an ASW surface should be adopted. If using a simpler model, which does not take into account the actual multilayer nature of the mantle, the diffusion between the different layers towards the surface must be accounted for. We could measure the desorption energy as a function of the ice thickness and select the energy corresponding to an average ice mantle thickness. This effective desorption energy that encompasses the diffusion can be directly implemented in such a simple model. We hypothesise that this effective value should be close to 31 kJ mol^{-1} as shown in Fig. 5 where we can see that the diffusion process retards the desorption of H_2CO. It is evident that the coupling between diffusion and desorption must be better understood. We have illustrated the extent to which studying diffusion within ASW is a necessary step towards that goal.

5. Conclusion

In this work we studied the desorption of H_2CO from different surfaces and demonstrated how its desorption is intrinsically linked to ASW in interstellar ices through trapping and reactivity. In the multilayer regime, bulk H_2CO ice desorbs following zeroth-order kinetics, which can be modelled using a Polanyi-Wigner equation with the parameters $\nu_0 = 10^{28} \pm 0$ molec cm^{-2} s^{-1} (fixed), $E = 31.3 \pm 0.5$ kJ mol^{-1}. In the submonolayer regime, H_2CO desorbs following first-order desorption kinetics. It is however simpler, and as accurate, to model this desorption as a zeroth-order desorption, employing the Polanyi-Wigner equation with the parameters $\nu_0 = 10^{28}$ mol cm^{-2} s^{-1} and $E = 27.1 +/- 0.5$ kJ/mol for the desorption from an ASW surface and with the parameters $\nu_0 = 10^{28}$ mol cm^{-2} s^{-1} (fixed) and $E = 31.0 +/- 0.9$ kJ/mol for a silicate surface.

The interaction of H_2CO with the ASW mantle is complex, as the desorption of H_2CO is linked with its diffusion in ASW, with its trapping inside the closed pore network of ASW (volcano desorption) and as hydrates (co-desorption with H_2O), and with the reactivity of H_2CO with H_2O. For slow temperature increases, as encountered in the interstellar medium, the reaction of H_2CO with H_2O is faster than its desorption, resulting in the production of the polymer polyoxymethylene. This study also highlights the importance of the diffusion process as it delays desorption and enables trapped molecules to encounter other molecules in the ice, increasing the probability of reactions occurring. Diffusion studies of small molecules within ASW must be undertaken in order to quantitatively account for the relationship between diffusion and desorption, and diffusion and reactivity.

Acknowledgements. J.N. wants to thank the Royal Commission for the Exhibition of 1851 for her fellowship.

References

Accolla, M., Congiu, E., Dulieu, F., et al. 2011, Phys. Chem. Chem. Phys., 13, 8037
Amiaud, L., Fillion, J. H., Baouche, S., et al. 2006, J. Chem. Phys., 124, 094702
Bossa, J. B., Theule, P., Duvernay, F., & Chiavassa, T. 2009, ApJ, 707, 1524
Barrie, P. J. 2012a, Phys. Chem. Chem. Phys., 14, 318
Barrie, P. J. 2012b, Phys. Chem. Chem. Phys., 14, 327
Boogert, A. C. A., Pontoppidan, K. M., Knez, C., et al. 2008, ApJ, 678, 985
Burke, D. J., & Brown, W. A. 2010, Phys. Chem. Chem. Phys., 12, 5947
Carter, V. 1962, Vacuum, 12, 245
Chazallon, B., Oancea, A., Capoen, B., & Focsa, C. 2008, Phys. Chem. Chem. Phys., 10, 702
Collings, M. P., Dever, J. W., Fraser, H. J., McCoustra, M. R. S., & Williams, D. A. 2003a, ApJ, 583, 1058
Collings, M. P., Dever, J. W., Fraser, H. J., & McCoustra, M. R. S. 2003b, Ap&SS, 285, 633
Collings, M. P., Anderson, M. A., Chen, R., et al. 2004, MNRAS, 354, 1133
Cronin, J. R., & Pizzarello, S. 1983, Adv. Space Res., 3, 5
Dartois, E. 2005, Space Sci. Rev., 119, 293
Draine, B. T. 2003, ARA&A, 41, 241
Fraser, H. J., Collings, M. P., McCoustra, M. R. S., & Williams, D. A. 2001, MNRAS, 327, 1165
Fuchs, G. W., Cuppen, H. M., Ioppolo, S., et al. 2009, A&A, 505, 629
Gerakines, P. A., Schutte, W. A., Greenberg, J. M., & van Dishoeck, E. F. 1995, A&A, 296, 810
Guzmán, V., Pety, J., Goicoechea, J. R., Gerin, M., & Roueff, E. 2011, A&A, 534, A49
Hiraoka, K., Ohashi, N., Kihara, Y., et al. 1994, Chemp. Phys. Lett., 229, 408
Keane, J. V., Tielens, A. G. G. M., Boogert, A. C. A., Schutte, W. A., & Whittet, D. C. B. 2001, A&A, 376, 254
Kimmel, G. A., Stevenson, K. P., Dohnálek, Z., Smith, R. S., & Kay, B. D. 2001, J. Chem. Phys., 114, 5284
Livingston, F. E., Smith, J. A., & George, S. M. 2002, J. Phys. Chem., 106, 6309
Maret, S., Ceccarelli, C., Caux, E., et al. 2004, A&A, 416, 577
Mayer, E., & Pletzer, R. 1986, Nature, 319, 298
Noble, J. A., Congiu, E., Dulieu, F., & Fraser, H. J. 2012, MNRAS, 421, 768
Nomura, H., & Millar, T. J. 2004, A&A, 414, 409
Milam, S. N., Remijan, A. J., Womack, M., et al. 2006, ApJ, 649, 1169
Öberg, K. I., Fayolle, E. C., Cuppen, H. M., van Dishoeck, E. F., & Linnartz, H. 2009, A&A, 505, 183
Palumbo, M. E. 2006, A&A, 453, 903
Palumbo, M. E., Baratta, G. A., Leto, G., & Strazzulla, G. 2010, J. Mol. Struct., 972, 64
Raut, U., Famá, M., Loeffler, M. J., & Baragiola, R. A. 2008, ApJ, 687, 1070
Redhead, P. A. 1962, Vacuum, 12, 203
Rowland, B., Fisher, M., & Devlin, J. P. 1991, J. Chem. Phys., 95, 1378
Smith, R. S., Huang, C., Wong, E. K. L., & Kay, B. D. 1997, Phys. Rev. Lett., 79, 909
Schutte, W. A., Allamandola, L. J., & Sandford, S. A. 1993, Icarus, 104, 118
Schutte, W. A., Gerakines, P. A., Geballe, T. R., van Dishoeck, E. F., & Greenberg, J. M. 1996, A&A, 309, 633
Theule, P., Duvernay, F., Ilmane, A., et al. 2011, A&A, 530, A96
Viti, S., & Williams, D. A. 1999, MNRAS, 305, 755
Viti, S., Collings, M. P., Dever, J. W., McCoustra, M. R. S., & Williams, D. A. 2004, MNRAS, 354, 1141
Watanabe, N., & Kouchi, A. 2002, ApJ, 571, L173
Wootten, A., Mangum, J., & Barsony, M. 1996, BAAS, 28, #105.08